Microturbulence in DIII-D tokamak pedestal. I. Electrostatic instabilities

D. P. Fulton,[1] Z. Lin,[1,2,a)] I. Holod,[1] and Y. Xiao[3]
[1]*Department of Physics and Astronomy, University of California, Irvine, California 92697, USA*
[2]*Fusion Simulation Center, Peking University, Beijing 100871, China*
[3]*Institute of Fusion Theory and Simulation, Zhejiang University, Hangzhou 310027, China*

(Received 6 November 2013; accepted 28 March 2014; published online 15 April 2014)

Gyrokinetic simulations of electrostatic driftwave instabilities in a tokamak edge have been carried out to study the turbulent transport in the pedestal of an H-mode plasma. The simulations use annulus geometry and focus on two radial regions of a DIII-D experiment: the pedestal top with a mild pressure gradient and the middle of the pedestal with a steep pressure gradient. A reactive trapped electron instability with a typical ballooning mode structure is excited by trapped electrons in the pedestal top. In the middle of the pedestal, the electrostatic instability exhibits an unusual mode structure, which peaks at the poloidal angle $\theta = \pm\pi/2$. The simulations find that this unusual mode structure is due to the steep pressure gradients in the pedestal but not due to the particular DIII-D magnetic geometry. Realistic DIII-D geometry appears to have a stabilizing effect on the instability when compared to a simple circular tokamak geometry. © *2014 AIP Publishing LLC*. [http://dx.doi.org/10.1063/1.4871387]

I. INTRODUCTION

The edge region of a tokamak plasma provides boundary conditions for the core and acts as a source of heat and particles to the scrape off layer (SOL), thus playing a crucial role in tokamak magnetic confinement fusion. One confinement regime, called the high-confinement mode or *H-mode*,[1] is characterized by steep gradients in both temperature and density in the edge region, with stiff core profiles. The area of steep gradients within the edge region is called the *pedestal* and provides a source of free energy which may drive a number of instabilities. Despite these instabilities, increased fusion gain and energy confinement make the H-mode a desirable operating scenario, a primary candidate for the ITER experiment,[2] and of general interest to the magnetic confinement community.

Manipulation of the pedestal and control of the H-mode require a strong theoretical understanding of edge physics and transport. Fine tuning H-mode confinement requires control of both pedestal temperature and density, which may be characterized by pedestal height and width. Limits on the pedestal height and width can be determined using empirical models.[3,4] Edge localized mode (ELM) cycles are observed experimentally; these cycles consist of initial pedestal growth, ELM build up, pedestal crash, and a return to pedestal growth/recovery.[5,6] Some research has been done to explore ELM onset and mitigation,[7–9] and one popular model to predict the onset of ELMs is peeling-ballooning theory.[10–12] Additionally, a large number of numerical simulations have been carried out and benchmarked against each other to study the peeling-ballooning mode linear instability.[13] Since it is desirable to tune H-mode confinement and, therefore, to tune pedestal parameters, the period of pedestal growth/recovery is of particular theoretical interest.

There are a number of unanswered questions regarding the pedestal recovery period in the ELMy cycle. The recovery period is typically long, on the order of tens of milliseconds. During this time period, low frequency magnetic fluctuations occur, called ELM precursors,[5,6,14] but the causal relationship between ELM precursors and ELMs is not yet fully understood. Possible candidates for ELM precursors are the kinetic ballooning mode (KBM) and resistive ballooning mode (RBM).[10,12] The KBM is a variant form of ideal ballooning mode (IBM) which includes kinetic effects: commonly diamagnetic effects and sometimes wave-particle interaction.[15] Both meso-scale MHD modes and micro-scale drift-Alfvènic modes should be included in a full picture of the pedestal recovery period. It is also unknown whether electrostatic or electromagnetic modes are primarily responsible for transport during the pedestal recovery. Electrostatic modes which may contribute significantly to the transport include the collisionless trapped electron mode (CTEM), dissipative trapped electron mode, and electrostatic interchange mode.[16]

To understand transport processes in the pedestal, we have initiated a series of gyrokinetic simulations for the drift-Alfvènic instabilities and associated microturbulence in a DIII-D H-mode pedestal. These simulations will proceed from electrostatic to electromagnetic and from linear to nonlinear. In this paper, we use gyrokinetic simulation to explore electrostatic instabilities driven by pressure gradients in the pedestal. Simulations are carried out using the Gyrokinetic Toroidal Code (GTC)[17] and based on DIII-D shot 131997 at time 3011 ms.[18] This work was initiated as part of the US Department of Energy Joint Research Target FY2011 to understand physics processes controlling the structure of the H-mode pedestal. To this end, a cross-code benchmark between gyrokinetic turbulence codes examined KBM stability in the pedestal. GTC annulus simulation finds a reactive trapped electron mode to be dominant at the top of the 131997 pedestal, sharing features with simulations from

a)Author to whom correspondence should be addressed. Electronic mail: zhihongl@uci.edu

other gyrokinetic codes, GYRO, GEM, and GS2.[19,20] In the steep gradient region, these drift instabilities are unusual in that they peak off the horizontal midplane at the poloidal angle $\theta = \pm\pi/2$, consistent with an earlier theory of a ballooning mode structure minimizing magnetic shear damping.[21,22] We demonstrate that this unusual mode structure is due to the steep pressure gradients in this region but not due to the specific magnetic geometry. In both the top of the pedestal and the steep gradient, we find that finite boundary conditions significantly affect instability growth rate and frequency. These findings motivate global simulations in future work.

The remainder of this paper is organized as follows: Section II details the simulation model. In Secs. III and IV, results are presented for the pedestal top and the steep gradient regions respectively. Discussion and interpretation of results occurs in Sec. V.

II. SIMULATION MODEL

For simulations presented in the current work, we use GTC's δf particle-in-cell implementation, with gyrokinetic ions and drift kinetic electrons.[23] GTC has been extensively applied to study turbulent transport in fusion plasmas including ion and electron temperature gradient modes,[24,25] collisionless trapped electron mode,[26] energetic particle transport,[27,28] and Alfvèn eigenmodes.[29,30] All of the simulations presented in this paper are electrostatic. The electrostatic version of the fluid-kinetic hybrid electron model[31] is used to efficiently treat electron dynamics.

Traditional gyrokinetic ordering[32,33] is well justified in the tokamak core region but not in the edge. In the edge, strong spatial inhomogeneities characterize the pedestal. A new ordering parameter, L_p, suitable for pedestal parameters, is considered in a recent gyrokinetic theory.[34] The resulting equations using this new ordering parameter are the same as when traditional gyrokinetic ordering is applied.[33] In this new ordering,

$$\frac{V_{\mathrm{E}}}{v_{\mathrm{th}}} \approx k_{\perp}\rho_i \frac{q_{\mathrm{i}}\delta\phi}{T} \sim \frac{\omega}{\Omega_{\mathrm{i}}} \sim \frac{\rho_i}{L_p} \sim \frac{L_p}{R} \sim \varepsilon \ll 1, \qquad (1)$$

where v_{th} is the thermal velocity, $k_{\perp}$ is the wavenumber perpendicular to the equilibrium magnetic field, ρ_i is the ion gyroradius, q_i is the charge of the main ion species, $\delta\phi$ is the perturbed electrostatic potential, T is the temperature, ω is the instability frequency, Ω_{i} is the ion cyclotron frequency, and R is the major radius. In Eq. (1), $V_{\mathrm{E}} = (c/B)\mathbf{b} \times \nabla\delta\phi$ is a characteristic drift velocity due to the turbulence, c is the sound speed, B is the magnitude of the magnetic field, and $\mathbf{b}$ is the unit vector in the direction of the magnetic field. The length scale L_p characterizes the strength of the gradients in the pedestal. For a radial function $f(r)$, the corresponding length scale is defined

$$\frac{1}{L_f} = \frac{1}{f(r)}\frac{d}{dr}f(r). \qquad (2)$$

At the steep gradient in DIII-D shot 131997, relevant pedestal quantities are the density (n) and ion and electron temperature (T_i and T_e respectively). In Table I, we compare the length scales of these three quantities to ρ_{i} and to the major radius on the magnetic axis (R_0).

The equilibrium used in this paper is based on DIII-D discharge 131997 at time 3011 ms. This discharge and others were originally part of an experiment to benchmark EPED, a predictive model of pedestal height and width constraints.[18] The intent in producing this equilibrium was to provide a good case for a gyrokinetic cross-code benchmark of KBM onset.[19,20] The equilibrium was generated from experimental measurements using varyped analysis and the EFIT equilibrium solver.[35] Time 3011 ms represents the discharge immediately prior to an ELM crash, when the peeling-ballooning mode would normally be expected to be near its stability threshold, however the peeling-ballooning drive was artificially reduced in this equilibrium in order to stabilize the peeling-ballooning mode and provide a good case for the KBM benchmark.

In Fig. 1, plasma profiles from the EFIT equilibrium are shown in a range $\psi_{\mathrm{n}} = [0.8, 1.0]$, where ψ_{n} is normalized poloidal flux. Throughout this paper, normalized poloidal flux is chosen to have a value $\psi_{\mathrm{n}} = 0$ at the magnetic axis, and normalized such that $\psi_{\mathrm{n}} = 1$ at the separatrix. The magnetic geometry is shown in Fig. 2. GTC simulations were done using this full DIII-D geometry, which is non-circular and up-down asymmetric. The simulations use the real electron-to-deuterium mass ratio which is 2.72309×10^{-4}. For simplicity, collisional effects are ignored in this work. Collisional effects may be relevant for the edge plasma, and will be reported in a future publication.

GTC is a global code with no implementation of local simulation or flux-tube boundary conditions. In the interest of benchmarking with local simulations, GTC non-local simulation treats only a narrow annulus in the poloidal plane in this work. For these annulus simulations, the full plasma profiles are replaced by constant-valued profiles taken from a local point of interest. Specifically, density and temperature values and their gradients are taken from the full equilibrium profiles at a single reference flux surface. These values are applied across the entire simulation domain. At radial boundaries, gradients are reduced to be zero. In this paper, simulations are run using parameters from two radial locations: at $\psi_{\mathrm{n}} = 0.95$, the top of the pedestal, and at $\psi_{\mathrm{n}} = 0.98$, the steep gradient region. These two locations are shown by the black dashed lines in Fig. 1. The full q profile and full magnetic geometry from EFIT are used. We emphasize that the difference between fixed radial boundary conditions in GTC annulus simulation and the typical periodic radial boundary condition of flux-tube simulations has a crucial effect on the simulation results.

TABLE I. Ordering parameters from DIII-D shot 131997 ($\psi_{\mathrm{n}} = 0.98$) satisfy gyrokinetic ordering (Eq. (1)).

ρ_i/L_n	ρ_i/L_{T_e}	ρ_i/L_{T_i}
6.47×10^{-2}	1.37×10^{-1}	4.48×10^{-2}
L_n/R_0	L_{T_e}/R_0	L_{T_i}/R_0
7.69×10^{-3}	3.64×10^{-3}	1.11×10^{-2}

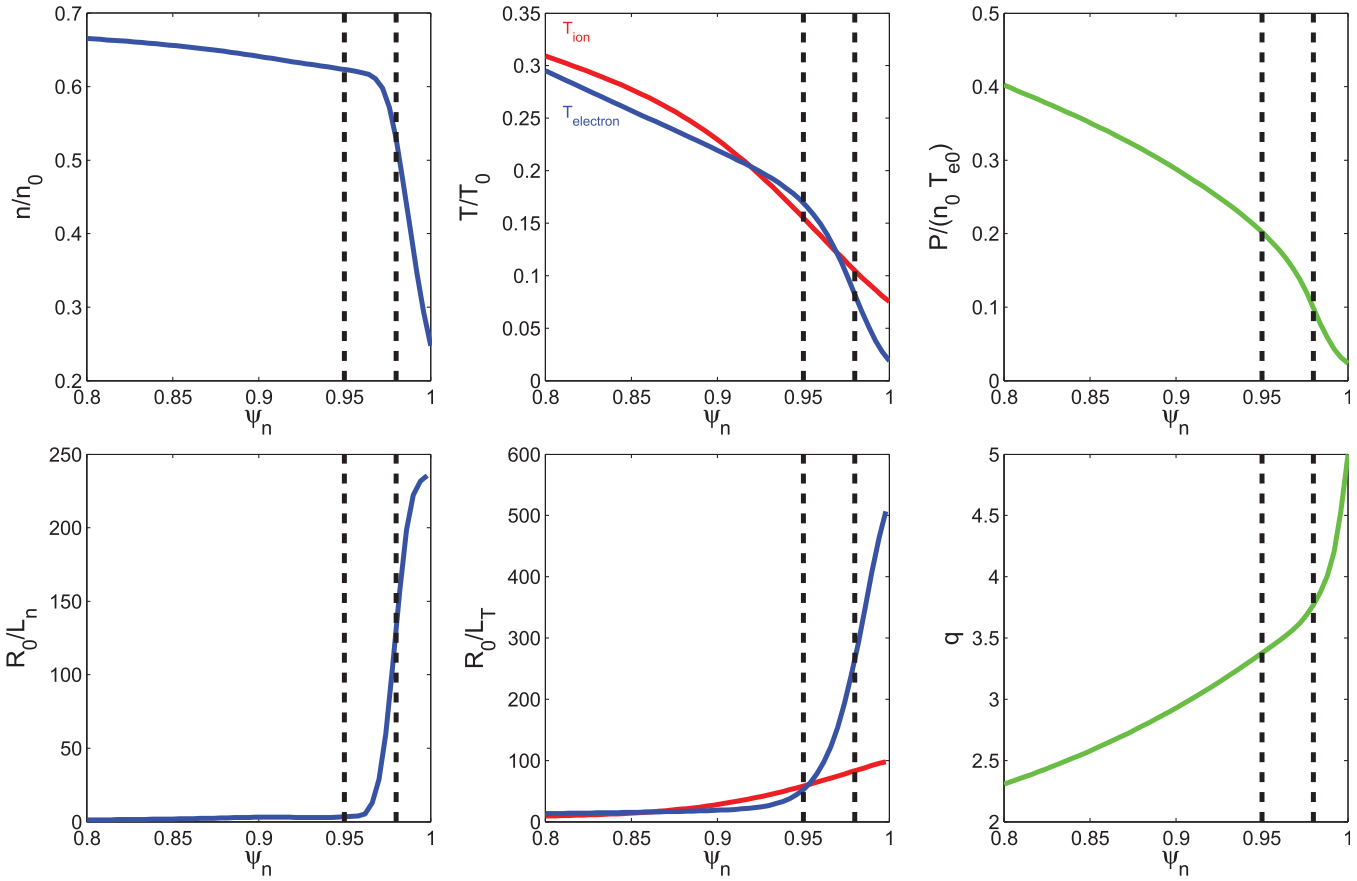

FIG. 1. Plasma profiles of DIII-D shot 131997, shown between normalized poloidal flux (ψ_n) values of 0.8 and 1.0. The top row, from left to right, shows density (n), ion and electron temperatures (T_i and T_e), and pressure (P), normalized to their magnetic axis values, denoted by subscript 0. The bottom row, from left to right, shows the inverse density length scale (R_0/L_n), the inverse ion and electron temperature length scales (R_0/L_{T_i} and R_0/L_{T_e}), and the safety factor (q). Red lines show ion quantities while blue show those of electrons. The vertical black dashed lines indicate the radial positions from which parameters were taken for the narrow annulus simulations.

III. PEDESTAL TOP

Initial GTC simulations used input parameters from the radial location $\psi_n = 0.95$, the pedestal top, where gradients are significantly less steep than in the middle of the pedestal. The ion and electron temperature gradients are strong here, while the density gradients are one to two orders of magnitude weaker. Fig. 3 shows instability frequency (ω_r) and growth rate (γ) over a scan of $k_\theta \rho_i$. As $k_\theta \rho_i$ increases, the magnitudes of both γ and ω_r also increase. The ratio of the instability frequency to growth rate is $|\omega_r|/|\gamma| \approx 0.65$ for $k_\theta \rho_i \approx 0.7$. A value of $|\omega_r|/|\gamma|$ less than one is characteristic of the reactive class of instabilities. The mode structure is broad in the poloidal coordinate, spanning the entire bad curvature region of the geometry. This mode structure is consistent with an interchange driven instability and in contrast to the more localized mode structure of a typical ballooning mode.[36] In order to understand how electron kinetic effects contribute to the instability, the simulation was repeated using a simpler adiabatic electron model. No instability was found when using only adiabatic electrons, indicating that trapped electrons provide the primary drive for the instability. This information leads us to more specifically identify the instability as a reactive trapped electron mode.[37] The simulation results shown in Figs. 3–5, include the kinetic electron model.

We can identify relevant wave-particle resonances which may excite the instability by examining various orbital frequencies. For a toroidal mode number $n = 42$ ($k_\theta \rho_i \approx 0.5$), the ratio of the electron diamagnetic drift frequency to the instability frequency, ω_e^*/ω_r is 33, and the ratio between the electron precession frequency and the instability frequency, $\omega_{pre,e}/\omega_r$ is approximately 1.4. Here, these frequencies are calculated, respectively, by $\omega_e^* = k_\theta \rho_e (v_{t,e}/L_n)$ and $\omega_{pre,e} = (nqT_e/eB_0 r R_0)$ where $v_{t,e}$ is the thermal electron velocity, e is the electron charge, and r is the minor radius. Primary energy exchange occurs through the electron toroidal precessional resonance.

As part of the cross-code benchmark effort, GEM and GYRO simulations also observe an electrostatic instability at the pedestal top.[19] GTC predicts a growth rate of only ~20% of the value predicted by GYRO and GEM flux-tube simulations. This difference is not surprising when considering that both the equilibrium and simulation model used by GTC are different than those used by GEM and GYRO during the benchmark. Two primary differences should be highlighted; First, as mentioned in Sec. II, GTC annulus simulations use a finite radial domain with fixed radial boundaries, while GEM and GYRO flux-tube simulations use a periodic radial boundary. Second, while the GTC simulations use a numerical representation of the real DIII-D geometry, GEM and

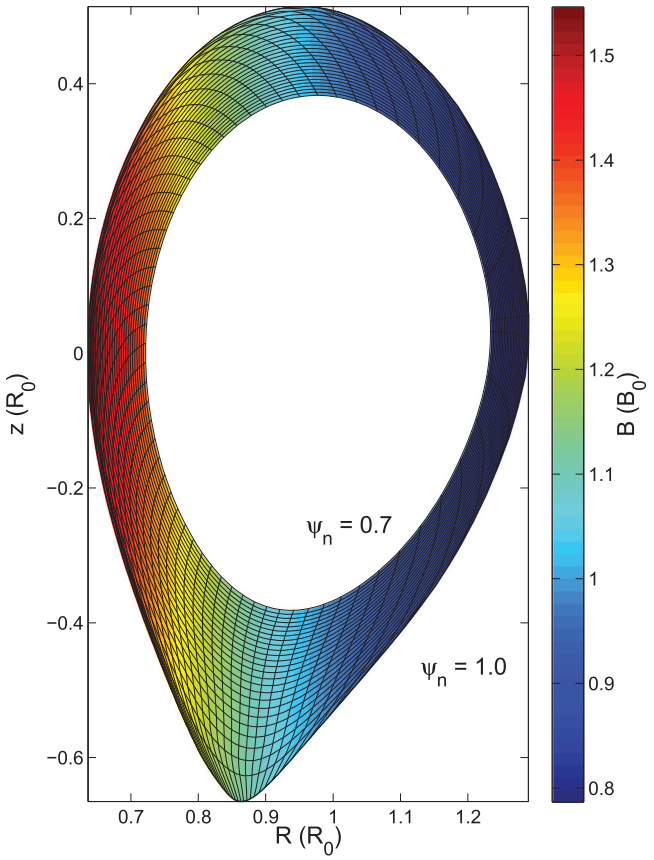

FIG. 2. DIII-D shot 131997 equlibrium geometry implemented in GTC annulus simulation for normalized poloidal flux $\psi_n = [0.7, 1.0]$. The color bar shows magnetic field strength (B) normalized to the value on the magnetic axis B_0.

GYRO use a parameterized Miller equilibrium fit to the realistic geometry. Miller parameterization is a good approximation of realistic geometry near the plasma core, but is unable to capture up-down asymmetry.[38] Because the equilibrium geometry for DIII-D shot 131997 is strongly up-down asymmetric in the pedestal, there is significant discrepancy between Miller geometry and realistic geometry in this case.

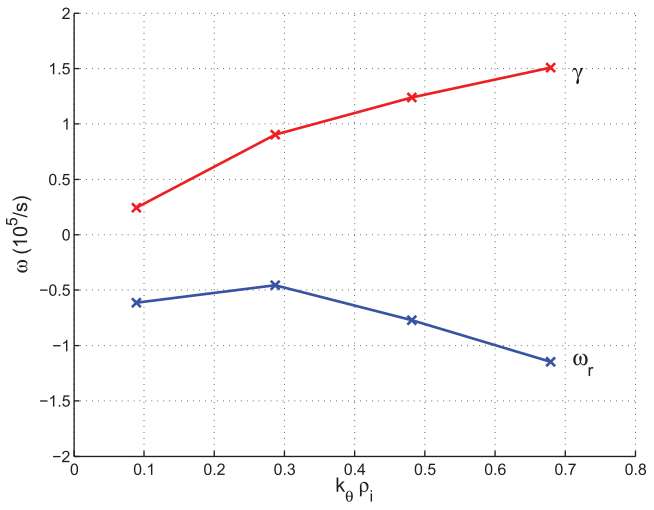

FIG. 3. Scan in $k_\theta \rho_i$ of growth rate (γ) and real frequency (ω_r) for "top of pedestal" $\psi_n = 0.95$ parameters.

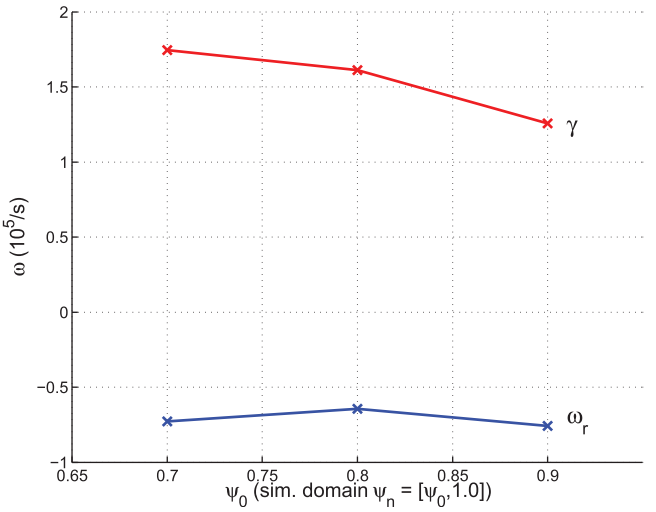

FIG. 4. Change of growth rate (γ) and real frequency (ω_r) versus inner boundary (ψ_0) of simulation domain for the top of pedestal ($\psi_n = 0.95$) simulation. All three cases have toroidal mode number $n = 42$ ($k_\theta \rho_i \sim 0.5$).

In order to test the boundary condition effects associated with the small radial domain size, GTC simulations were executed with three different-sized annuli, from [0.7, 1.0], [0.8, 1.0], and [0.9, 1.0] in ψ_n. Physically, this changes the geometry, since the global realistic geometry is used in all cases. The free energy available to drive the mode is also increased as the extent of the strong pressure gradient is increased. All three cases were run for $k_\theta \rho_i \approx 0.5$, or toroidal mode number, $n = 42$. Fig. 4 shows a reduction of the growth rate by approximately 30% as the annulus size is reduced, indicating that boundary condition effects are significant. The electrostatic potential in the poloidal plane, shown in Fig. 5, in all three cases exhibits typical ballooning structure that peaks on the outboard midplane at $\theta = 0$, where θ is the poloidal angle. As the radial domain is reduced across the three cases in Fig. 5, the mode structure becomes visibly narrowed.

IV. STEEP GRADIENT REGION

For this case, we chose a location in the center of the plasma pedestal at $\psi_n = 0.98$. Electrostatic GTC annulus simulation captures a driftwave instability. The mode structure has the unusual characteristic of being peaked away from the outboard midplane.

Using the steep gradient parameters, both a scan of toroidal mode number and a boundary condition domain-size test were carried out using GTC. Shown in Fig. 6, both γ and ω_r at $\psi_n = 0.98$ increase with $k_\theta \rho_i$. Poloidal mode structure across the scan is qualitatively consistent (Fig. 8). In contrast to the top of pedestal case, the real frequency is now positive in the electron diamagnetic direction. As in the top of pedestal case, the mode has the characteristic of a reactive type instability; The magnitude of the real frequency is small compared to that of the growth rate. For toroidal mode number $n = 25$ ($k_\theta \rho_i \approx 0.25$), the ratio of the electron diamagnetic drift frequency to the instability frequency, ω_e^*/ω_r is approximately 7.8, and the ratio of the electron precession frequency to the instability frequency is $\omega_{pre,e}/\omega_r \sim 0.20$.

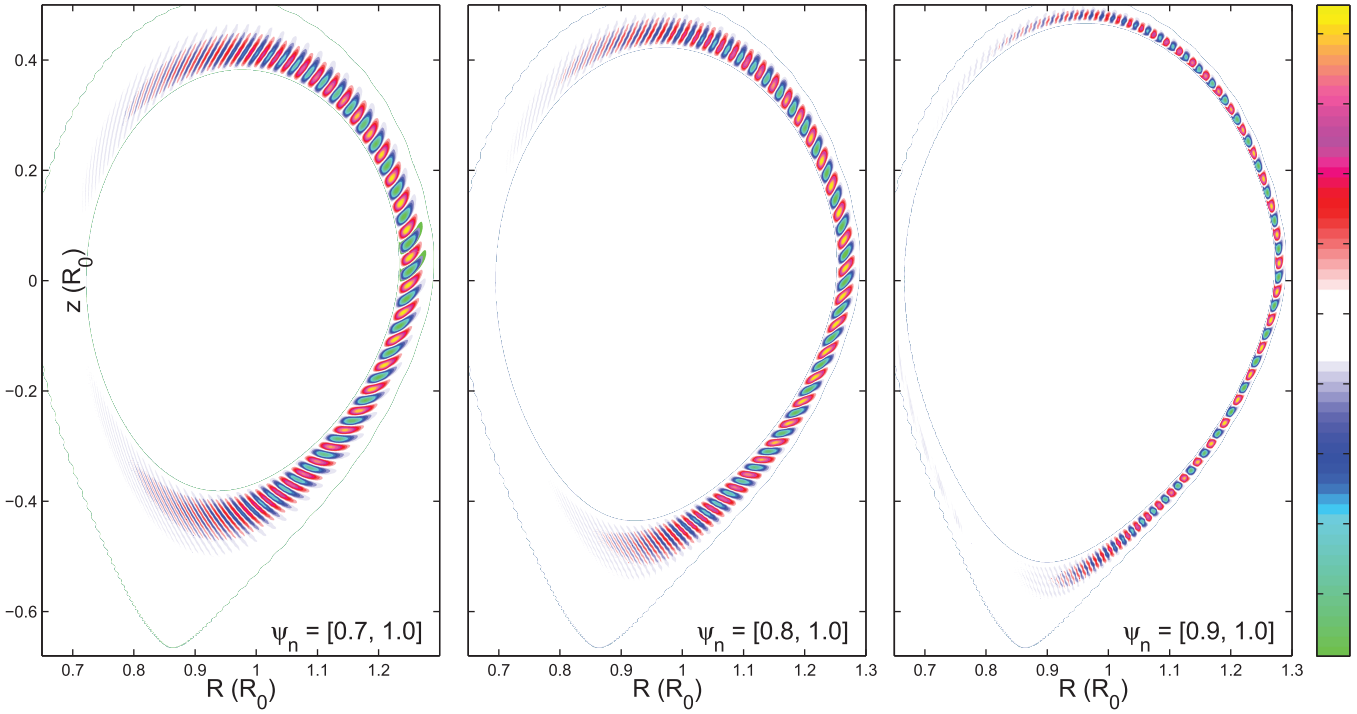

FIG. 5. Poloidal mode structure of electrostatic potential (ϕ) for simulations with three different annulus sizes using profile parameters from the top of pedestal ($\psi_n = 0.95$) in the DIII-D experiment. All three cases have toroidal mode number $n = 42$ ($k_\theta \rho_i \sim 0.5$).

Fig. 7 shows the instability frequency and growth rate for the four cases used in the domain-size scan with steep gradient parameters. The four different sized annuli used in this scan span [0.7, 1.0], [0.8, 1.0], [0.9, 1.0], and [0.95, 1.0] in ψ_n. The real frequency changes significantly as the radial domain is varied, while the growth rate remains approximately constant (Fig. 7). As before, by extending the simulation box size, we are affecting both the geometry and the drive of instability. Fig. 8 shows the mode structure of the electrostatic potential in the poloidal plane, for the three narrowest annulus cases.

A simulation using only an adiabatic electron model was also carried out for $n = 25$, yielding no instability. This result indicates that trapped electrons provide the primary instability drive for the steep gradient case. The figures in this section all show results from simulations using the kinetic electron model.

In the narrowest annulus case with $\psi_n = [0.95, 1.0]$, the radial simulation domain is only $\approx 9\rho_i$, which may contribute to numerical inaccuracy. To assess this possibility, we artificially reduce the ion mass by a factor of four, effectively increasing the simulation domain size relative to ρ_i. Reducing the ion mass by a factor of four reduces ρ_i by a

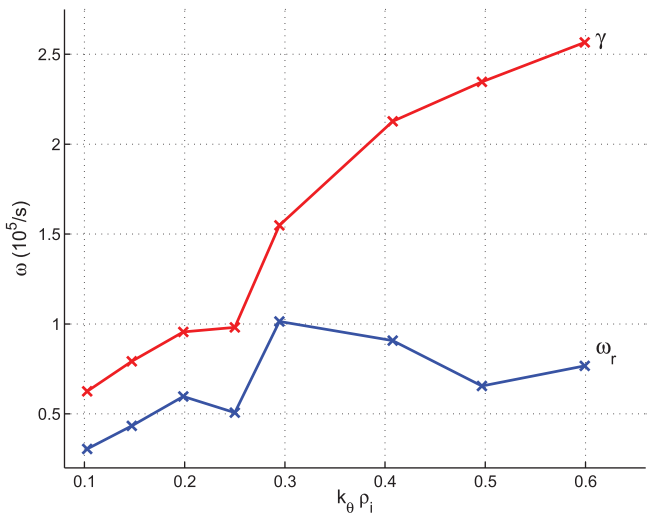

FIG. 6. Scan in $k_\theta \rho_i$ of growth rate (γ) and real frequency (ω_r) for "steep gradient" $\psi_n = 0.98$ parameters.

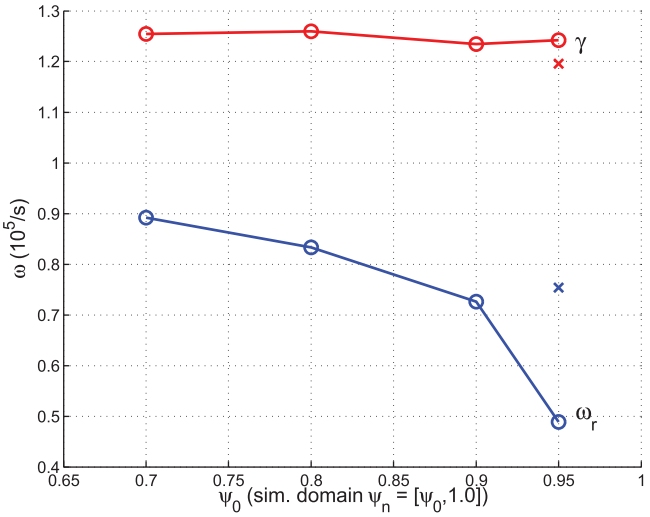

FIG. 7. Change of growth rate (γ) and real frequency (ω_r) versus inside boundary (ψ_0) of simulation domain, for steep gradient ($\psi_n = 0.98$) simulation. The points indicated by "x" show simulation results for identical geometry and plasma profiles, but with ion mass reduced by a factor of four. This mass reduction halves the Larmor radius, effectively increasing the simulation domain size. All cases have toroidal mode number $n = 25$ (regular mass $k_\theta \rho_i \sim 0.25$; reduced mass $k_\theta \rho_i \sim 0.125$).

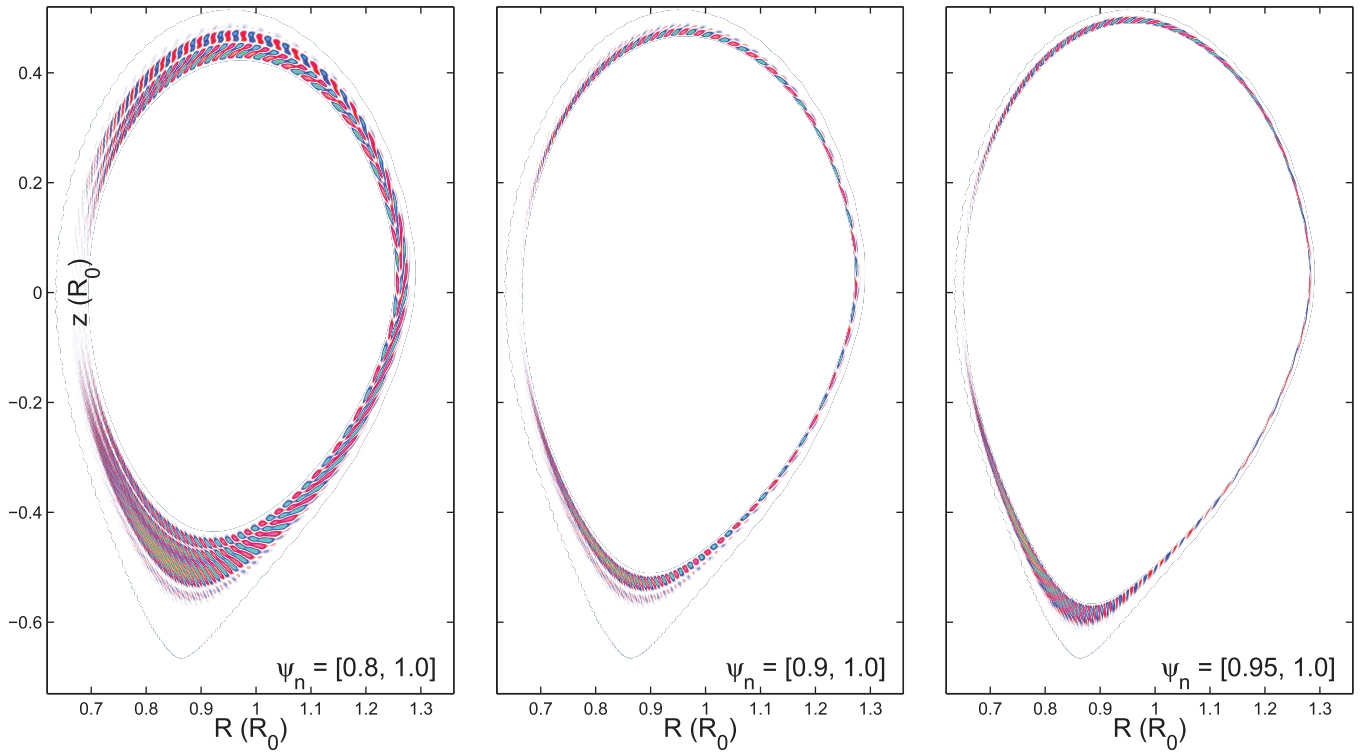

FIG. 8. Poloidal mode structure of electrostatic potential (ϕ) for simulations with three different radial domains. Profiles and gradients use values from the steep gradient region $(\psi_n = 0.98)$ of the DIII-D experiment. All three cases have toroidal mode number $n = 25$ $(k_\theta \rho_i \sim 0.25)$.

factor of two, and the simulation domain becomes approximately $18\rho_i$ in size. The results from the reduced mass simulation are shown in Fig. 7 by the "x" markers. The real frequency of the reduced mass case is approximately 80% of the real frequency of [0.7, 1.0] normal mass case, while the [0.95, 1.0] normal mass case is approximately 55%.

The drop in real frequency with narrowing of simulation domain is alleviated in the reduced mass simulations. This reduction indicates that the small ratio between the simulation domain size and ρ_i is primarily responsible for the drop in real frequency across the non-local scan. The growth rate is reduced by approximately 5% in the reduced mass simulation.

Unlike a typical ballooning mode structure, which peaks at the outboard midplane $(\theta \approx 0)$, the electrostatic potential in the poloidal plane in Fig. 8 has a peak near the top and bottom of the plane $(\theta \approx \pm\pi/2)$. This feature appears in both simulations with the original deuterium mass as well as with the scaled down mass. Existing theory demonstrates that mode peaking at $\theta = \pm\pi/2$ may occur along with up-down symmetry breaking in the poloidal plane. Analytic theory using simplified geometry and equilibria has demonstrated this effect by using an alternate form of the ballooning transformation.[22] GYRO flux-tube simulations in benchmark efforts also produced off-midplane mode peaking using local parameters from the steep gradient location and demonstrated that this feature may be produced by scaling the gradient scale lengths of density and temperature from the top of pedestal values to the steep gradient values.[19] Recent GEM simulations of a DIII-D H-mode pedestal also find turbulence concentrated at the bottom of the poloidal plane.[39]

Multiple GTC simulations using reduced density and temperature gradients demonstrate that off midplane mode peaking is a result of strong pressure gradients and not the unique geometry of DIII-D shot 131997. In order to separate the gradient and geometry effects, both gradient strength and geometry are varied in GTC simulations. The gradient values of density, ion temperature, and electron temperature are taken from the full equilibrium profiles at $\psi_n = 0.98$. These three gradient values are then multiplied by the same constant factor to produce a scaled gradient case. Four cases were tested, using constant factors 0.1, 0.2, 0.5, and 1.0, corresponding to 10%, 20%, 50%, and 100% of experimental gradient values. These four cases are carried out for two distinct geometries: a realistic, numerical DIII-D geometry (Fig. 2), and a simplified circular tokamak geometry.

In Fig. 9, mode structures of the electrostatic potential are shown for the three strongest drive cases using the DIII-D geometry. Fig. 10 shows the mode amplitudes, radially and toroidally averaged and normalized to their outboard midplane value, versus the poloidal angle (θ). These two figures show the mode structures for the 10% and 20% gradient cases peaking at $\theta = 0$, as is characteristic of typical ballooning modes. The 50% and 100% gradient mode structures display the off-midplane mode-peaking at $\theta = \pm\pi/2$.

The same four simulations are carried out using a simple tokamak with concentric flux surfaces. For this circular geometry case, plasma profiles and gradients as a function of ψ_n are identical to the experimental geometry case. The results of the circular tokamak simulation are shown in Figs. 11 and 12. Again, typical ballooning structure is seen for 10% and 20% gradient cases, while off-midplane mode

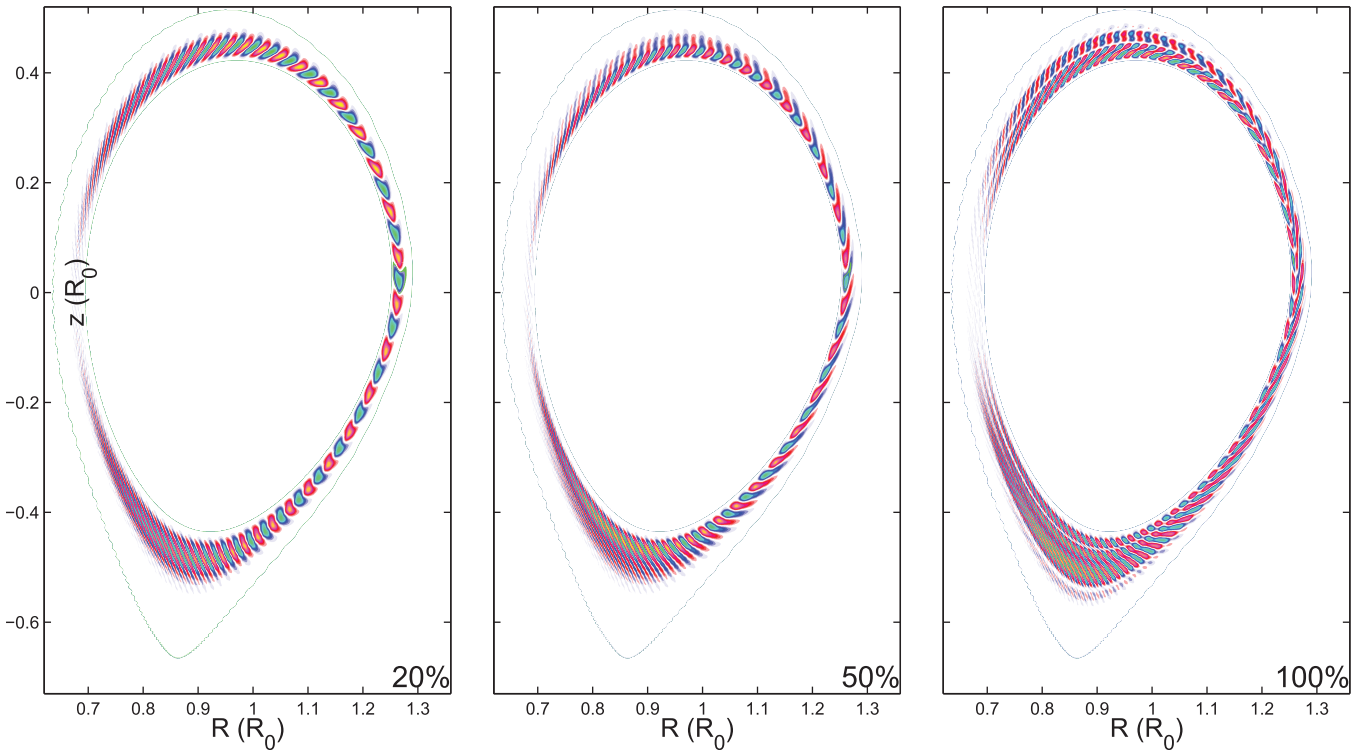

FIG. 9. Poloidal mode structure of electrostatic potential (ϕ) is shown for varying values of density and temperature gradients for DIII-D geometry simulations. From left to right the 20%, 50%, and 100% gradient cases are shown. All cases use a radial domain $\psi_n = [0.8, 1.0]$.

peaking is seen for the stronger 50% and 100% gradient cases.

The feature of off-midplane mode-peaking appears in both DIII-D geometry and circular tokamak cases, thus appearing to be independent of geometry. Real frequencies and growth rates for gradient scans in each geometry are shown in Fig. 13 and demonstrate that the DIII-D geometry has a stabilizing effect when compared to the circular tokamak geometry. As expected for pressure gradient driven modes, Fig. 13 shows increased growth rate as the pressure gradient is increased. The geometry appears to have negligible effect on the real frequency of the instability.

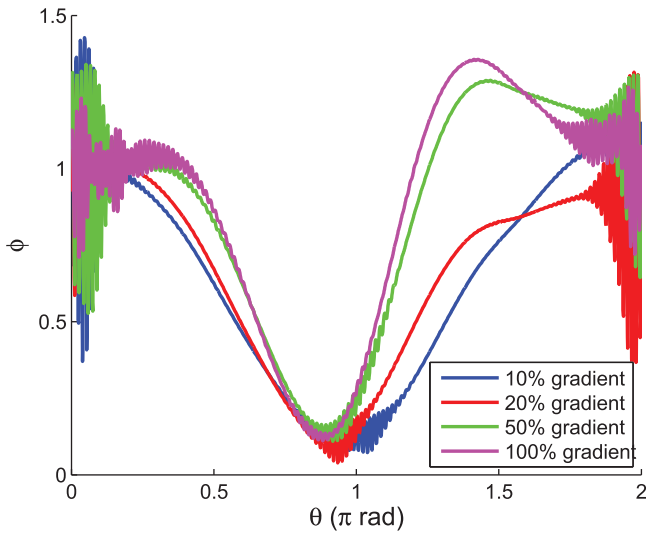

FIG. 10. Mode amplitude of electrostatic potential (ϕ), averaged over radial and toroidal coordinates and normalized to $\theta = 0$ value, versus poloidal angle (θ) for DIII-D geometry simulation at steep gradient $(\psi_n = 0.98)$.

V. DISCUSSION

In this study, gyrokinetic simulation with local parameters in a narrow annulus domain is used to explore electrostatic instabilities in the pedestal of DIII-D discharge 131997. A reactive trapped electron mode with typical ballooning characteristics (peaking at the outer midplane) is found using parameters from the top of pedestal location. This is in qualitative agreement with results from GEM and GYRO simulations carried out as part of benchmark efforts.

In the steep gradient region of the pedestal, a qualitatively different mode structure, characterized by off-midplane mode peaking, was observed in simulation. By artificially reducing gradient strength from experimental values for both realistic DIII-D and simplified circular tokamak geometry, we verify that this effect is due to the strength of the pedestal pressure gradients, but not an effect of DIII-D's particular experimental geometry. Realistic DIII-D geometry appears to have a stabilizing effect on the instability when compared to the simple circular tokamak. In all cases, varying the extent of the simulation domain, well outside the extent of the pedestal, affects either the growth rate or the real frequency, motivating global GTC simulations.

The ultimate goal of pedestal simulations is to understand the transport in the edge plasma. To this end, nonlinear simulation is critical. Possible contributors to turbulence regulation in nonlinear simulation are zonal flow, zonal field, and the geodesic acoustic mode (GAM).[36,40] In correspondence to the finding that boundary condition effects are

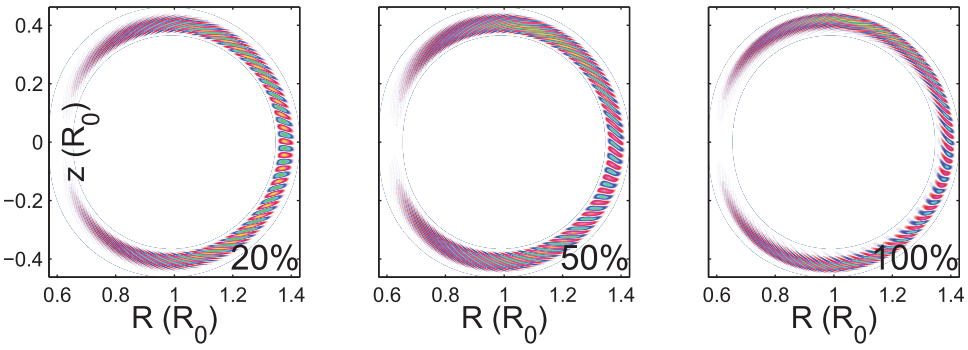

FIG. 11. Poloidal mode structure of electrostic potential (ϕ) for varying values of density and temperature gradients for a simple tokamak model with circular flux surfaces. From left to right the 20%, 50%, and 100% gradient cases are displayed. All cases use a radial domain $\psi_n = [0.8, 1.0]$.

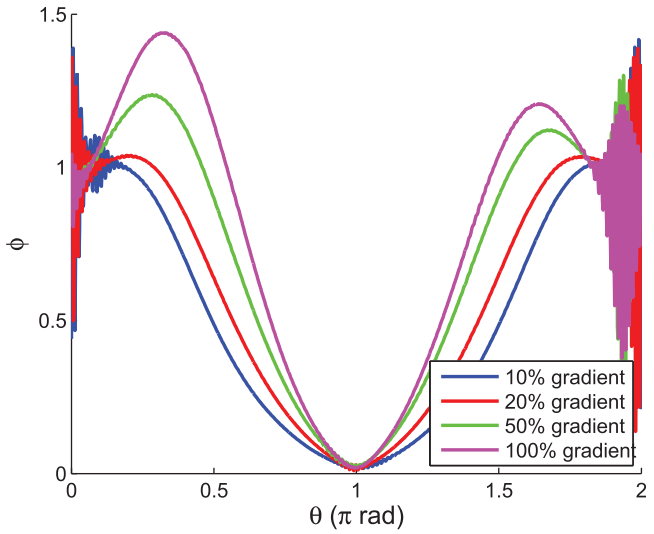

FIG. 12. Mode amplitude of electrostatic potential (ϕ), averaged over radial and toroidal coordinates and normalized to $\theta = 0$ value, versus poloidal angle (θ) for circular tokamak geometry simulation at steep gradient ($\psi_n = 0.98$).

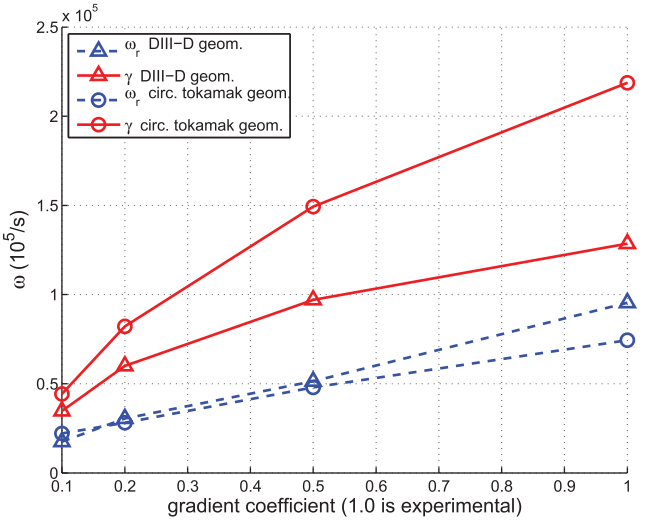

FIG. 13. Frequency (ω_r) and growth rate (γ) versus gradient strength for DIII-D and circular tokamak geometries using steep gradient ($\psi_n = 0.98$) parameters.

important in this region, more realistic global simulations using full plasma profiles and gradients will be included in future work. To determine whether electrostatic or electromagnetic modes are dominant in the edge, electromagnetic simulations will also be necessary in the future. All simulations up to this point have assumed a collisionless plasma, but we would like to understand the importance of collisionality in the pedestal in future studies.

ACKNOWLEDGMENTS

The authors would like to thank Richard Groebner, Philip Snyder, and Jeff Candy from General Atomics for providing EFIT equilibrium data on DIII-D discharge 131997 at time 3011 ms as well as their insights during benchmark efforts. We are also grateful for ongoing discussion with Eric Wang and Xueqiao Xu at LLNL and Weigang Wan, Scott Parker, and Yang Chen from the GEM group at University of Colorado, Boulder. This work was supported by U.S. DOE Grant Nos. DE-SC0010416 and DE-FG02-07ER54916, and China National Magnetic Confinement Fusion Science Program Grant Nos. 2013GB111000 and 2011GB105001. This research used resources of the Oak Ridge Leadership Computing Facility at Oak Ridge National Laboratory (DOE Contract No. DE-AC05-00OR22725), and the National Energy Research Scientific Computing Center (DOE Contract No. DE-AC02-05CH11231).

[1]F. Wagner, G. Becker, K. Behringer, D. Campbell, A. Eberhagen, W. Engelhardt, G. Fussmann, O. Gehre, J. Gernhardt, G. v. Gierke, G. Haas, M. Huang, F. Karger, M. Keilhacker, O. Klüber, M. Kornherr, K. Lackner, G. Lisitano, G. G. Lister, H. M. Mayer, D. Meisel, E. R. Müller, H. Murmann, H. Niedermeyer, W. Poschenrieder, H. Rapp, H. Röhr, F. Schneider, G. Siller, E. Speth, A. Stäbler, K. H. Steuer, G. Venus, O. Vollmer, and Z. Yü, "Regime of improved confinement and high beta in neutral-beam-heated divertor discharges of the ASDEX tokamak," Phys. Rev. Lett. **49**(19), 1408 (1982).
[2]See http://www.iter.org for ITER—the way to new energy.
[3]P. B. Snyder, N. Aiba, M. Beurskens, R. J. Groebner, L. D. Horton, A. E. Hubbard, J. W. Hughes, G. T. A. Huysmans, Y. Kamada, A. Kirk, C. Konz, A. W. Leonard, J. Lönnroth, C. F. Maggi, R. Maingi, T. H. Osborne, N. Oyama, A. Pankin, S. Saarelma, G. Saibene, J. L. Terry, H. Urana, and H. R. Wilson, "Pedestal stability comparison and ITER pedestal prediction," Nucl. Fusion **49**(8), 085035 (2009).
[4]P. B. Snyder, R. J. Groebner, J. W. Hughes, T. H. Osborne, M. Beurskens, A. W. Leonard, H. R. Wilson, and X. Q. Xu, "A first-principles predictive model of the pedestal height and width: development, testing and ITER optimization with the EPED model," Nucl. Fusion **51**(11), 103016 (2011).
[5]H. Zohm, "Edge localized modes (ELMs)," Plasma Phys. Controlled Fusion **38**, 105–128 (1996).
[6]J. W. Conner, "Edge-localized modes—physics and theory," Plasma Phys. Controlled Fusion **40**, 531–542 (1998).
[7]S. J. Fielding, P. G. Carolan, J. W. Conner, N. J. Conway, A. R. Field, P. Helander, Yu. Igitkhanov, B. Lloyd, H. Meyer, A. W. Morris, O. Pogutse, M. Valovi, and H. R. Wilson, "Transition dynamics and confinement scaling in COMPASS-D H mode plasmas," Nucl. Fusion **41**(7), 909–917 (2001).

[8]P. T. Lang, G. D. Conway, T. Eich, L. Fattorini, O. Gruber, S. Günter, L. D. Horton, S. Kalvin, A. Kallenbach, M. Kaufmann, G. Kocsis, A. Lorenz, M. E. Manso, M. Maraschek, V. Mertens, J. Neuhauser, I. Nunes, W. Schneider, W. Suttrop, and H. Urano, "ELM pace making and mitigation by pellet injection in ASDEX upgrade," Nucl. Fusion **44**(5), 665–677 (2004).
[9]T. E. Evans, R. A. Moyer, K. H. Burrel, M. E. Fenstermacher, I. Joseph, A. W. Leonard, T. H. Osborne, G. D. Porter, M. J. Schaffer, P. B. Snyder, P. R. Thomas, J. G. Watkins, and W. P. West, "Edge stability and transport control with resonant magnetic perturbations in collisionless tokamak plasmas," Nature Phys. **2**(6), 419–423 (2006).
[10]J. W. Conner, R. J. Hastie, H. R. Wilson, and R. L. Miller, "Magnetohydrodynamic stability of tokamak edge plasmas," Phys. Plasmas **5**(7), 2687–2700 (1998).
[11]P. B. Snyder, H. R. Wilson, J. R. Ferron, L. L. Lao, A. W. Leonard, T. H. Osborne, A. D. Turnbull, D. Mossessian, M. Murakami, and X. Q. Xu, "Edge localized modes and the pedestal: A model based on coupled peeling-ballooning modes," Phys. Plasmas **9**(5), 2037–2043 (2002).
[12]H. R. Wilson, P. B. Snyder, G. T. A. Huysmans, and R. L. Miller, "Numerical studies of edge localize instabilities in tokamaks," Phys. Plasmas **9**(4), 1277–1286 (2002).
[13]B. J. Burke, S. E. Kruger, C. C. Hegna, P. Zhu, P. B. Snyder, C. R. Sovinec, and E. C. Howell, "Edge localized linear ideal magnetohydrodynamic instability studies in an extended-magnetohydrodynamic code," Phys. Plasmas **17**(3), 032103 (2010).
[14]A. Loarte, G. Saibene, R. Sartori, D. Campbell, M. Becoulet, L. Horton, T. Eich, A. Herrmann, G. Matthews, N. Asakura, A. Chankin, A. Leonard, G. Porter, G. Federici, G. Janeschitz, M. Shimada, and M. Sugihara, "Characteristic of type I ELM energy and particle losses in existing devices and their extrapolation to ITER," Plasma Phys. Controlled Fusion **45**(9), 1549–1569 (2003).
[15]F. Zonca, L. Chen, J. Q. Dong, and R. A. Santoro, "Existence of ion temperature gradient driven shear Alfvèn instabilities in tokamaks," Phys. Plasmas **6**(5), 1917–1924 (1999).
[16]W. Horton, "Drift waves and transport," Rev. Mod. Phys. **71**(3), 735–778 (1999).
[17]Z. Lin, T. S. Hahm, W. W. Lee, W. M. Tang, and R. B. White, "Turbulent transport reduction by zonal flows: massively parallel simulations," Science **281**, 1835 (1998).
[18]R. J. Groebner, A. W. Leonard, P. B. Snyder, T. H. Osborne, C. F. Maggi, M. E. Fenstermacher, C. C. Petty, and L. W. Owen, "Progress towards a predictive model for pedestal height in DIII-D," Nucl. Fusion **49**(8), 085037 (2009).
[19]E. Wang, X. Xu, J. Candy, R. J. Groebner, P. B. Snyder, Y. Chen, S. E. Parker, W. Wan, Gaimin Lu, and J. Q. Dong, "Linear gyrokinetic analysis of a DIII-D H-mode pedestal near the ideal ballooning threshold," Nucl. Fusion **52**(10), 103015 (2012).
[20]R. J. Groebner, C. S. Chang, J. W. Hughes, R. Maingi, P. B. Snyder, X. Q. Xu, J. A. Boedo, D. P. Boyle, J. D. Callen, J. M. Canik, I. Cziegler, E. M. Davis, A. Diallo, P. H. Diamond, J. D. Elder, D. P. Eldon, D. R. Ernst, D. P. Fulton, M. Landreman, A. W. Leonard, J. D. Lore, T. H. Osborne, A. Y. Pankin, S. E. Parker, T. L. Rhodes, S. P. Smith, A. C. Sontag, W. M. Stacey, J. Walk, W. Wan, E. H.-J. Wang, J. G. Watkins, A. E. White, D. G. Whyte, Z. Yan, E. A. Belli, B. D. Bray, J. Candy, R. M. Churchill, T. M. Deterly, E. J. Doyle, M. E. Fenstermacher, N. M. Ferraro, A. E. Hubbard, I. Joseph, J. E. Kinsey, B. LaBombard, C. J. Lasnier, Z. Lin, B. L. Lipschultz, C. Liu, Y. Ma, G. R. McKee, D. M. Ponce, J. C. Rost, L. Schmitz, G. M. Staebler, L. E. Sugiyama, J. L. Terry, M. V. Umansky, R. E. Waltz, S. M. Wolfe, L. Zeng, and S. J. Zweben, "Improved understanding of physics processes in pedestal structure, leading to improved predictive capability for ITER," Nucl. Fusion **53**(9), 093024 (2013).
[21]J. W. Conner, J. B. Taylor, and H. R. Wilson, "Shear damping of drift waves in toroidal plasmas," Phys. Rev. Lett. **70**(12), 1803–1805 (1993).
[22]T. Xie, Y. Z. Zhang, S. M. Mahajan, and A. K. Wang, "Ballooning theory of the second kind–two dimensional tokamak modes," Phys. Plasmas **19**, 072105 (2012).
[23]I. Holod, W. L. Zhang, Y. Xiao, and Z. Lin, "Electromagnetic formulation of global gyrokinetic particle simulation in toroidal geometry," Phys. Plasmas **16**(12), 122307 (2009).
[24]Z. Lin, I. Holod, L. Chen, P. H. Diamond, T. S. Hahm, and S. Ethier, "Wave-particle decorrelation and transport of anisotropic turbulence in collisionless plasmas," Phys. Rev. Lett. **99**(26), 265003 (2007).
[25]Z. Lin, S. Ethier, T. S. Hahm, and W. M. Tang, "Verification of gyrokinetic particle simulation of device size scaling of turbulent transport," Plasma Sci. Technol. **14**(12), 1125–1126 (2012).
[26]Y. Xiao and Z. Lin, "Turbulent transport of trapped-electron modes in collisionless plasmas," Phys. Rev. Lett. **103**(8), 085004 (2009).
[27]W. Zhang, Z. Lin, and L. Chen, "Transport of energetic particles by microturbulence in magnetized plasmas," Phys. Rev. Lett. **101**(9), 095001 (2008).
[28]W. Zhang, Z. Lin, and L. Chen, "Comment on 'Electrostatic and magnetic transport of energetic ions in turbulent plasmas'," Phys. Rev. Lett. **107**(23), 239501 (2011).
[29]H. S. Zhang, Z. Lin, and I. Holod, "Nonlinear frequency oscillation of Alfvèn Eigenmodes in fusion plasmas," Phys. Rev. Lett. **109**(2), 025001 (2012).
[30]Z. Wang, Z. Lin, I. Holod, W. W. Heidbrink, B. Tobias, M. Van Zeeland, and M. E. Austin, "Radial localization of toroidicity-induced Alfvèn eigenmodes," Phys. Rev. Lett. **111**(14), 145003 (2013).
[31]Z. Lin, Y. Nishimura, Y. Xiao, I. Holod, W. L. Zhang, and L. Chen, "Global gyrokinetic particle simulations with kinetic electrons," Plasma Phys. Controlled Fusion **49**, B163 (2007).
[32]W. W. Lee, "Gyrokinetic approach in particle simulation," Phys. Fluids **26**(2), 556–562 (1983).
[33]A. J. Brizard and T. S. Hahm, "Foundations of nonlinear gyrokinetic theory," Rev. Mod. Phys. **79**(2), 421 (2007).
[34]A. M. Dimits, "Gyrokinetic equations for strong-gradient regions," Phys. Plasmas **19**(2), 022504 (2012).
[35]L. L. Lao, J. R. Ferron, R. J. Groebner, W. Howl, H. St. John, E. J. Strait, and T. S. Taylor, "Equilibrium analysis of current profiles in tokamaks," Nucl. Fusion **30**(6), 1035 (1990).
[36]F. Liu, Z. Lin, J. Q. Dong, and K. J. Zhao, "Gyrokinetic simulation of turbulence driven geodesic acoustic modes in edge plasmas of HL-2A tokamak," Phys. Plasmas **17**(11), 112318 (2010).
[37]T. A. Davydova, J. Weiland, and A. I. Yakimenko, "Shear velocity stabilization of reactive trapped electron modes," Phys. Plasmas **9**(11), 4623–4632 (2002).
[38]R. L. Miller, M. S. Chu, J. M. Greene, Y. R. Lin-Liu, and R. E. Waltz, "Noncircular, finite aspect ratio, local equilibrium model," Phys. Plasmas **5**(4), 973–978 (1998).
[39]W. Wan, S. E. Parker, Y. Chen, R. J. Groebner, and Z. Yan, "Global gyrokinetic simulations of the H-mode tokamak edge pedestal," Phys. Plasmas **20**(5), 055902 (2013).
[40]K. Hallatschek and D. Biskamp, "Transport control by coherent zonal flows in the core/edge transitional regime," Phys. Rev. Lett. **86**(7), 1223–1226 (2001).